Solution-processed Au–Ag core–shell nanoparticle-decorated yarns for human motion monitoring†

Hyung Ju Park,[a] Wan-Joong Kim,[a] Chil Seong Ah,[a] Yongseok Jun[b] and Yong Ju Yun*[b]

Wearable strain sensors based on Au–Ag core–shell nanoparticle decorated yarns were fabricated by a solution-based approach. Smart wearable systems with our strain sensors that can monitor various human motions, including finger motion, marching and squatting, and transmit the information of human motion in real time to an LED light was demonstrated.

Introduction

Flexible/wearable strain sensors are critical technologies in wearable electronics because of their diverse applications from biomedical applications to soft robotics.[1] To date, several groups have demonstrated many applications of wearable electronics for sensing human motions on both small scales (frequency pressures with breathing and eye movement) and large scales (finger motions and various leg motions including walking, running, and jumping), as well as for remote controlled devices.[2–11] Although a variety of wearable strain sensors have been developed, several limitations remain for their widespread use, including high-cost processing requirements with micro-fabrication processes, complicated steps, and slow production. Thus, a facile route with solution-based processes that can easily be scaled up is highly desired.

Electronic textiles (e-textiles) have been extensively developed for wearable electronics applications such as electrical interconnectors, battery and solar cell electrodes, physical and chemical sensors, and electric generators due to their soft nature, light weight, and low costs.[12–19] In particular, fiber-shaped e-textiles can be knit, woven, and braided into textiles or garments of various forms.[20,21] Moreover, unlike other flexible/wearable devices, most e-textiles can be fabricated solely *via* solution-based and continuous processes without the need for vacuum microfabrication.

Here, we made Au–Ag core–shell cotton yarns (AuAgCSCYs) with good properties by simple dip-coating of small size controlled gold nanoparticles on the surface of a cotton yarn, followed by an electroless and cheap silver deposition. And we

developed highly flexible and sensitive strain sensors based on the AuAgCSCYs; we then demonstrate a wearable system integrated with our strain sensors that can monitor a diverse range of human motions. Strain sensors were fabricated by employing both simple dipping and chemical reactions without vacuum processing. These core–shell yarns exhibit high sensitivity (gauge factor = 20) and possess good mechanical stability under 500 repetitive bending cycles at a maximum bending radius of 1 mm. Moreover, these flexible and durable strain sensors could be integrated into textiles or commercial cloth in various forms. We also demonstrated that these wearable systems with our flexible and sensitive strain sensors could monitor finger motions and leg motions (marching in place and body weight squatting).

Experimental sections

1. Synthesis of AuNPs

Gold nanoparticles (AuNPs) were prepared by following a previously reported procedure with slight modifications.[22] In a 500 mL round-bottomed flask equipped with a reflux condenser, 355 mL of water was boiled while being stirred vigorously. A 5 mL aqueous solution containing 158 mg of $HAuCl_4 \cdot 3H_2O$ was added to the boiling water. When the resulting solution was re-boiled, 40 mL of an aqueous solution containing 235.3 mg trisodium citrate dihydrate was added to the solution. The final concentrations of $HAuCl_4 \cdot 3H_2O$ and trisodium citrate dihydrate were 1 mM and 4 mM, respectively. The mixture was refluxed for another 10 min and allowed to cool to room temperature. The resulting solution of colloidal particles was characterized by an absorption maximum at 515 nm (Fig. S2c in the ESI†). Further spectral analysis indicated a particle diameter of 13 nm and a concentration of $\sim 5 \times 10^{-9}$ M (Fig. S2a–c in the ESI†).

2. Preparation of the AuCYs

Prior to the chemical modification of commercial CYs, the CYs were washed several times with water and ethanol. To form the

[a]Electronics and Telecommunications Research Institute (ETRI), Daejeon 34129, Republic of Korea

[b]Department of Energy Engineering, Konkuk University, Seoul 05029, Republic of Korea. E-mail: yjjun@konkuk.ac.kr

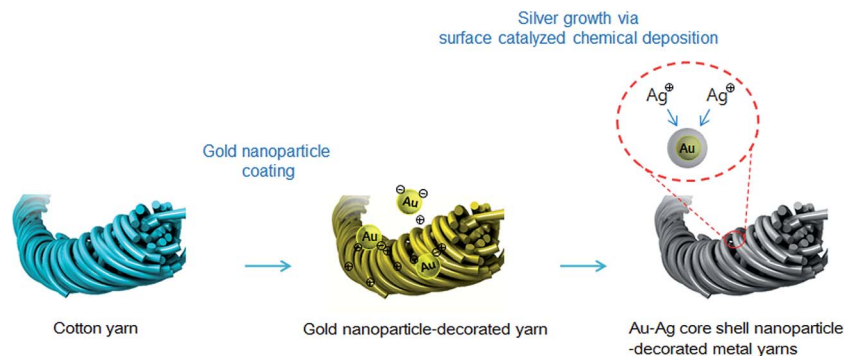† Electronic supplementary information (ESI) available. See DOI: 10.1039/c6ra26860a

Fig. 1   Schematic illustration for fabricating the AuAgCSCY strain sensor.

amine-terminated self-assembled layers on the CYs surfaces, the CYs were subsequently immersed in a 5% (v/v) APTES aqueous solution for 1 h at room temperature; the solution containing CYs and APTES was then stirred vigorously. After the functionalization of amine groups on the CYs surface, the AuNPs were covalently immobilized onto the CYs surface by immersing the amine terminated CYs in the synthesized gold colloidal solution for 24 h. The AuCYs were confirmed by analyzing scanning electron microscopy (SEM) and transmission electron microscopy (TEM) images, and energy dispersive X-ray (EDX) spectra (Fig. S3 and S4a in the ESI†).

3.   Preparation of the AuAgCSCYs

After washing with pure water, the AuCYs were immersed with 50 mL aqueous solution of 11.7 mM $AgNO_3$ aqueous solution. Then the AuAgCSCYs were prepared by adding 50 mL of 45.4 mM hydroquinone reduction agent solution, and the solution was vigorously stirred at room temperature for 10 min. The AgAuCSCYs were confirmed by analyzing SEM and TEM images, and EDX spectrum (Fig. 2b–e and S4b in ESI†).

4.   Characterization

The morphology and material elements of all samples were obtained by field emission scanning electron microscopy (FE-SEM, JEOL-6701F, JEOL Company, JAPAN) equipped with an EDX system and field emission transmission electron microscopy (200 kV FE-TEM, JEM-2100F, JEOL Company, JAPAN). UV-visible extinction measurements were performed using a SHI-MADZU UV-2501PC spectrometer over a wavelength range of 300–800 nm. Electrical conductance was measured using a two-point probe setup.

5.   Flexible and durability test

Electromechanical properties of the samples as a function of bending cycle number were measured by repeatedly bending and releasing the samples using a home-made electromechanical test machine. Samples that were 2 cm in width underwent repetitive bending–releasing for over 1000 cycles, and the electrical resistance was simultaneously recorded. All tests were performed at various bending angles (9°, 28°, 64°, 72°) with a scan rate of 1.0 mm s^{-1}.
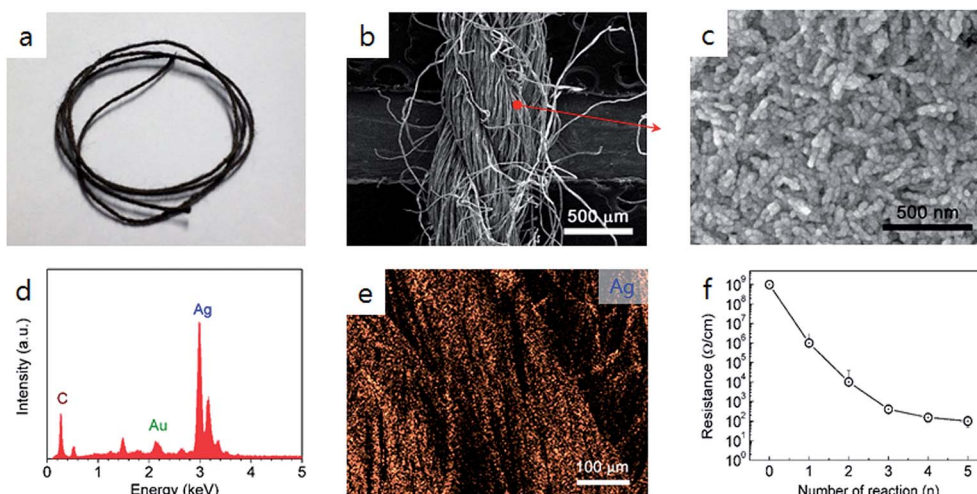

Fig. 2   Flexible AuAgCSCY strain sensor. (a) Optical image of core−shell yarns. (b) SEM image of core−shell yarns. (c) Enlarged high-resolution SEM image of (b). (d and e) EDX spectrum analysis and corresponding Ag mapping of core−shell yarns. (f) Resistance as a function of the number of silver-growing. The average resistance per centimeter of samples were calculated over ten specimens for each sample and error bars for standard deviation are shown.

6. Wearable system for monitoring human motions

Wearable glove and knee pad system consists of the AuAgCSY strain sensor, commercial glove and knee pad, a micro-controller (Arduino Uno), conducting thread, light emitting diode (LED) and power source (9 V battery) (see Fig. S5 in the ESI†).

Results and discussion

Fig. 1 illustrates the key processes in fabricating the AuAgCSCYs for strain sensing. These core–shell yarns were formed in two consecutive steps: (i) cotton yarns (CYs) were decorated with gold nanoparticles *via* a simple dipping process, and then (ii) AuAgCSCYs were obtained by silver growth *via* surface catalyzed chemical growth. First, commercial CYs were used as templates and 13 nm citrate-stabilized gold nanoparticles were used as precursors for fabricating the gold nanoparticle-decorated CYs (AuCYs) (Fig. S1 and S2 in the ESI†). A thin citrate layer on the surface nanoparticles made them negatively charged.[23] The CYs were functionalized with 3-aminopropyltriethoxysilane (APTES) to induce a positive charge on the yarn surface. The as-prepared amine-functionalized CYs were dipped into an aqueous gold nanoparticle solution with a low pH (3–4) for 24 h. A uniform coating of negative charged gold nanoparticles was formed on the amine-functionalized CYs through electrostatic self-assembly (Fig. 1, center). FESEM and TEM images, and energy dispersive X-ray (EDX) spectra of the AuCYs revealed that gold nanoparticles were uniformly coated on the CY surfaces (Fig.

S3a and b and S4a in the ESI†). For the AuAgCSCYs, $AgNO_3$ was employed as a precursor with hydroquinone as a reducing agent. The positive charged silver ions can attach onto the surface of negative charged gold nanoparticles through electrostatic interactions. Thin Ag shells are formed on the surface of the AuCYs through the reduction of silver ions with hydroquinone (Fig. 1, left). Further fabrication process details and characterization are provided in the methods and ESI.†

Representative AuAgCSCYs are presented in Fig. 2a. After silver growth, the CY color changed from dark purple to dark gray (Fig. S1†). Fig. 2b shows SEM images of the AuAgCSCYs with an average diameter of 800 μm and its enlarged SEM image shows Au–Ag core–shell particles on the surface of the CY, indicating the successful deposition of silver on the AuCYs surface (Fig. 2c). After silver deposition *via* the surface catalyzed chemical reaction, the EDX spectra exhibited typical Au–Ag core–shell particles spectral features, such as a Au peak at 2.13 keV and a Ag peak at 2.98 keV (Fig. 2d). Compared to the EDX spectra of plain AuCYs, the EDX intensity of Ag peak was significantly increased here, revealing that Ag nanoparticles were uniformly distributed on the AuCY surfaces (Fig. S3b in the ESI†). The uniform distribution of Ag on the AuAgCSCYs is confirmed by EDX elemental mapping as shown in Fig. 2e, where Ag is uniformly distributed throughout the AuAgCSCYs. Fig. 2f shows the electrical resistance changes of the AuAgCS-CYs as measured by a two probe method as a function of the amount of silver present. Initially-prepared AuCYs composed of citrate-stabilized gold nanoparticles have insulator-like
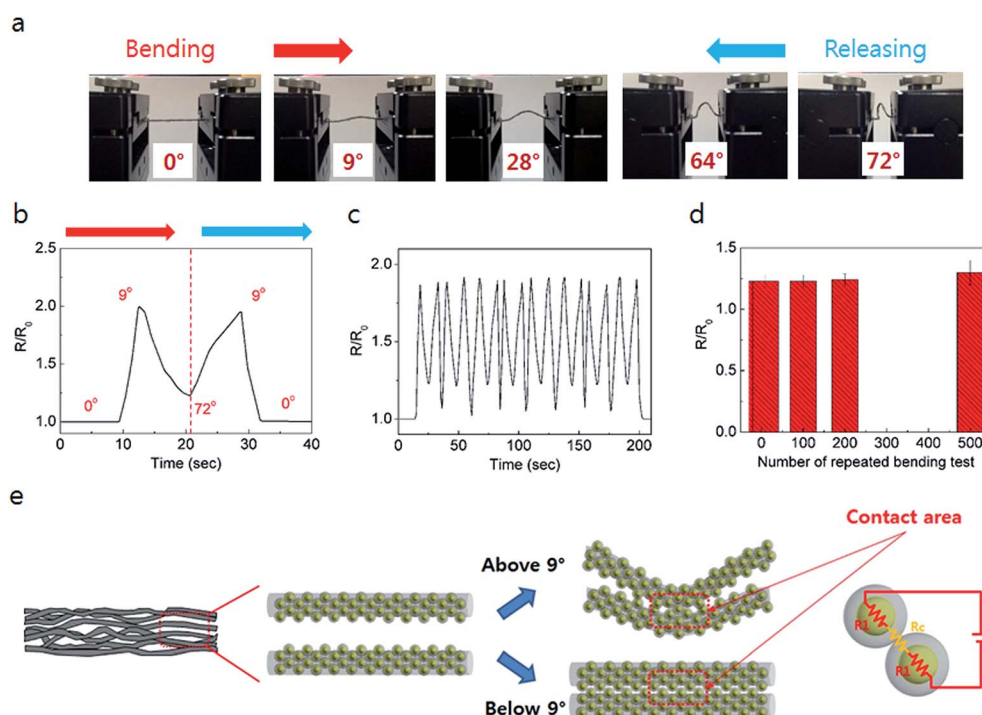
Fig. 3 Electromechanical properties of the AuAgCSCY strain sensor. (a) Photograph images of the AuAgCSCYs under 0°, 9°, 28°, 64°, 72°. (b) Variation in resistance of the sensor under bending–releasing. (c) Variation in resistance of the sensor under repeated bending–releasing at 72°. (d) Mechanical durability test of the sensor under repeated bending–releasing at 72° (500 cycles). (e) Schematic illustration of strain sensing mechanism of the Au–Ag core–shell nanoparticles-decorated yarns.

behavior owing to the high contact resistance and charge carrier scattering between nanoparticles. As the amount of deposited silver increases, the electrical resistance rapidly decreases from 1 GΩ cm^{-1} ($n = 0$) to 500 Ω cm^{-1} ($n = 3$) and reached a minimum value of 90 Ω cm^{-1} at $n = 5$. In addition, oxidation and Ag$^+$ release of the Au–Ag core–shell particles in the presence of oxygen can play an important role in their antibacterial activities. So we think that it can also be used as self-cleaning flexible materials.[24–26]

The relative resistance variation was recorded in order to determine the flexible properties of the AuAgCSCYs. We evaluated their flexibility by measuring the resistance while changing the bending angle from 0° to 72° (Fig. 3a). Fig. 3b shows their resistance variation (R/R_0, where R is the measured resistance and R_0 is the original electrical resistance before bending) as a function of bending angle. This plot could be divided into two linear regions with different resistance changes and slope. Notably, their resistance values increase until 9° and then abruptly decrease from 9° to 72°. The slope of the resistance change reflects the gauge factor (GF), which is defined as ($\Delta R/R$)/($\Delta L/L$), where R is the electrical resistance and L is the length of the strain sensor. For bending from 0° to 9°, the relative change in the AuAgCSCY resistance increased by a factor of 2.0 (GF: 20). For bending angles over 9°, the relative change in the resistance decreased by a factor of 0.6 (GF: −2.7). The value of GF for bending angles <9° was approximately 10 times greater than that for bending >9°. This difference in GF reveals that there are two different mechanisms affecting the resistance under deformation, as shown in Fig. 3e. This schematic explains the mechanism underlying the change in the resistance for the two

ranges of bending. In the initial bending phase below 9°, the increase in resistance is caused by a decrease in the contact area between individual core–shell nanoparticles coated cotton microfibers. When the yarn is bent beyond 9°, individual conducting microfibers begin to attach at the center region (Fig. 3e). Therefore, the change in the electrical resistance can be attributed to the contacts between microfibers during the bending and stretching processes.

The durability and stability of the strain sensor are very important factors for practical applications. To investigate the long-term stability, 500 repeated cycles of bending and releasing (with a bending radius of 1 mm) were applied to the sensor. The resistance remains unchanged even after performing 100 bending cycles at a maximum bending radius of 1 mm (similar to a 72° bending angle) and only increases by about 5% after 500 stretching cycles (Fig. 3d), which indicates the excellent durability and stability of the device under deformation. The outstanding sensitivity and stability of the AuAgCSCYs strain sensor made it possible to detect or monitor diverse human body activities, such as finger motions and leg motions (marching in place and body weight squatting).

To demonstrate the potential of the AuAgCSCYs as strain sensors in wearable electronics, we fabricated strain sensor-integrated wearable systems for monitoring human finger and leg motions. The wearable systems were composed of our strain sensors, microcontroller, conducting thread, light-emitting diode (LED), and a commercial glove (Fig. S5 in the ESI†). Fig. 4a presents a glove integrated with a AuAgCSCYs strain sensor for finger motion monitoring. To facilitate attachment and release of the strain sensor from the glove, the ends of the
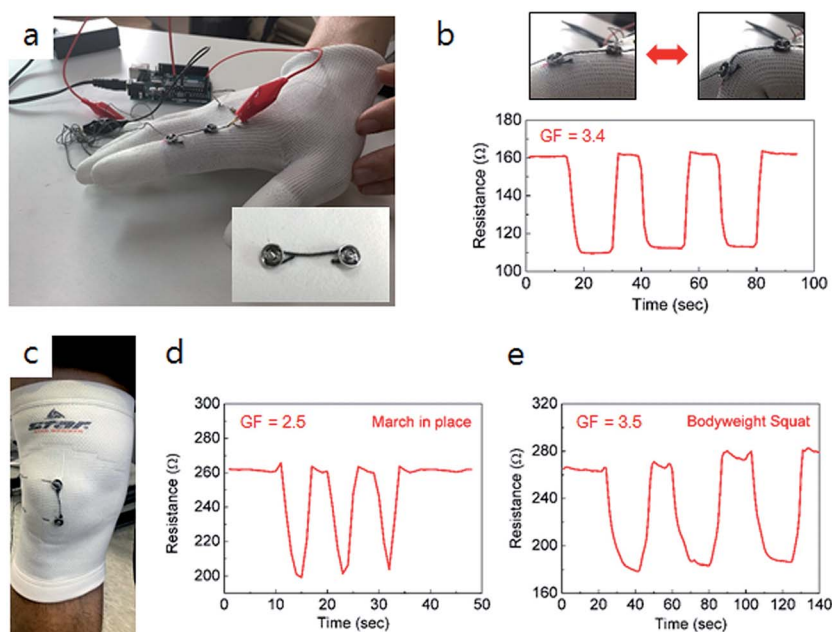

Fig. 4 Applications of the AuAgCSCYs strain sensor. (a) Photograph of wearable glove system with one strain sensor. Inlet: image of the strain sensor. (b) Relative changes in resistance *versus* time for various finger motions. Inset: photographs of the sensor assembled to an index finger for motion measurement. (c) Photograph of wearable pad system. (d and e) Relative changes in resistance *versus* time while marching in place and bodyweight squatting for strain sensors placed over a knee joint.

AuAgCSCYs were connected to snap fasteners (inset of Fig. 4a). By assembling the sensor into an index finger, finger motions could be monitored by measuring resistance changes associated with variations in the degree of finger bending (Fig. 4b). The upper insets show bent or released fingers, and the resistance variation was recorded in real time during the bending process. In the initial bending position, the finger was flexed, causing the sensor to stretch and its relative resistance to decrease. During the bending motion, the sensor stretched and bent with the joint, causing the relative change in resistance to decrease. Upon returning back to the initial position, the relative change of resistance returned back to the baseline. The sensor responded to the finger motions with good sensitivity and repeatability. Additionally, to clarify the selectivity of the strain sensor to other type of deformation, we measured the relative change in resistance under finger abduction. The strain sensor was repeatedly twisted while measuring resistance (Fig. S6†). The relative change in resistance was ~4.4%. This result demonstrate that the strain sensor has a high sensitivity under other types of deformations. Due to its superior ability to detect finger joint motions, this wearable glove system enables this finger motion information to be transmitted in real time to an attached LED. As demonstrated in Movie S1 (ESI†), the wearer's finger motion was continuously monitored using a strain sensor, and the information successfully displayed. Fig. 4c–e demonstrate the potential of the wearable strain sensors to monitor leg movement. We fabricated a wearable system made from one AuAgCSCYs strain sensor assembled on a knee pad (Fig. 4c). When the sensor unit was fixed to the knee joint, diverse leg motions such as marching and squatting could be monitored (Fig. 4d and e). These results demonstrate that the AuAgCSCYs strain sensor has great potential for monitoring a diverse range of human movements. This device and system could be used as a medical device to monitor patient and athlete motions, or as a smart hand to remotely control robotics such as drones.

Conclusions

In conclusion, we have developed a new wearable strain sensor with high sensitivity and good durability that can record a diverse range of human motions, which can also be integrated into textiles or garments. Moreover, these devices were fabricated solely using solution-based and continuous processes without the use of vacuum conditions. We believe that this method opens a pathway for the low-cost and large-scale fabrication of new flexible materials and wearable devices for future technologies involving smart wearable systems for use in healthcare and biomedical systems, sports, entertainment and other areas.

Acknowledgements

References

1 N. Lu and D.-H. Kim, *Soft Robotics*, 2014, **1**, 53–62.
2 D. Kang, P. V. Pikhitsa, Y. W. Choi, C. Lee, S. S. Shin, L. Piao, B. Park, K.-Y. Suh, T.-i. Kim and M. Choi, *Nature*, 2014, **516**, 222–226.
3 D.-H. Kim, N. Lu, R. Ma, Y.-S. Kim, R.-H. Kim, S. Wang, J. Wu, S. M. Won, H. Tao, A. Islam, K. J. Yu, T.-i. Kim, R. Chowdhury, M. Ying, L. Xu, M. Li, H.-J. Chung, H. Keum, M. McCormick, P. Liu, Y.-W. Zhang, F. G. Omenetto, Y. Huang, T. Coleman and J. A. Rogers, *Science*, 2011, **333**, 838–843.
4 C. Pang, G.-Y. Lee, T.-i. Kim, S. M. Kim, H. N. Kim, S.-H. Ahn and K.-Y. Suh, *Nat. Mater.*, 2012, **11**, 795–801.
5 Y. Wang, L. Wang, T. Yang, X. Li, X. Zang, M. Zhu, K. Wang, D. Wu and H. Zhu, *Adv. Funct. Mater.*, 2014, **24**, 4666–4670.
6 S. Lee, Y. Inoue, D. Kim, A. Reuveny, K. Kuribara, T. Yokota, J. Reeder, M. Sekino, T. Sekitani, Y. Abe and T. A. Someya, *Nat. Commun.*, 2014, **5**, 5898, DOI: 10.1038/ncomms6898.
7 Q. Li, Z. Ullah, W. Li, Y. Guo, J. Xu, R. Wang, Q. Zeng, M. Chen, C. Liu and L. Liu, *Small*, 2016, **36**, 5058–5065.
8 T. Yamada, Y. Hayamizu, Y. Yamamoto, Y. Yomogida, A. Izadi-Najafabadi, D. N. Futaba and K. Hata, *Nat. Nanotechnol.*, 2011, **6**, 296–301.
9 J. Lee, S. Kim, J. Lee, D. Yang, B. C. Park, S. Ryu and I. Park, *Nanoscale*, 2014, **6**, 11932–11939.
10 J. D. Pegan, J. Zhang, M. Chu, T. Nguyen, S.-J. Park, A. Paul, J. Kim, M. Bachman and M. Khine, *Nanoscale*, 2016, **8**, 17295–17303.
11 S. Jung, J. H. Kim, J. Kim, S. Choi, J. Lee, I. Park, T. Hyeon and D.-H. Kim, *Adv. Mater.*, 2014, **26**, 4825–4830.
12 L. M. Castano and A. B. Flatau, *Smart Mater. Struct.*, 2014, **23**, 053001.
13 K. Jost, C. R. Perez, J. K. McDonough, V. Presser, M. Heon, G. Dion and Y. Gogotsi, *Energy Environ. Sci.*, 2011, **12**, 5060–5067.
14 S. Ryu, P. Lee, J. B. Chou, R. Xu, R. Zhao, A. J. Hart and S.-G. Kim, *ACS Nano*, 2015, **9**, 5929–5936.
15 C. Wang, X. Li, E. Gao, M. Jian, K. Xia, Q. Wang, Z. Xu, T. Ren and Y. Zhang, *Adv. Mater.*, 2016, **17**, 6640–6648.
16 X. Wu, Y. Han, X. Zhang and C. Lu, *ACS Appl. Mater. Interfaces*, 2016, **8**, 9936–9945.
17 Y. J. Yun, W. G. Hong, N.-J. Choi, B. H. Kim, Y. Jun and H.-K. Lee, *Sci. Rep.*, 2015, **5**, 10904, DOI: 10.1038/srep10904.
18 J. J. Park, W. J. Hyun, S. C. Mun, Y. T. Park and O. O. Park, *ACS Appl. Mater. Interfaces*, 2015, **7**, 6317–6324.
19 W. Seung, M. K. Gupta, K. Y. Lee, K.-S. Shin, J.-H. Lee, T. Y. Kim, S. Kim, J. Lin, J. H. Kim and S.-W. Kim, *ACS Nano*, 2015, **9**, 3501–3509.
20 W. Zeng, L. Shu, Q. Li, S. Chen, F. Wang and X.-M. Tao, *Adv. Mater.*, 2014, **26**, 5310–5336.

21 W. Weng, P. Chen, S. He, X. Sun and H. Peng, *Angew. Chem., Int. Ed.*, 2016, **55**, 6140–6169.

22 J. J. Storhoff, R. Elghanian, R. C. Mucic, C. A. Mirkin and R. L. Letsinger, *J. Am. Chem. Soc.*, 1998, **120**, 1959–1964.

23 C. A. Mirkin, *Inorg. Chem.*, 2000, **39**, 2258–2272.

24 B. L. Ouay and F. Stellacci, *Nano Today*, 2015, **10**, 339–354.

25 Q. Liu, Z. Zhou, G. Qiu, J. Li, J. Xie and J. Y. Lee, *ACS Sustainable Chem. Eng.*, 2015, **3**, 2959–2966.

26 L. Zhang, Y. He, N. Goswami, J. Xie, B. Zhang and X. Tao, *Chemosphere*, 2016, **153**, 322–331.